九州大学学術情報リポジトリ
Kyushu University Institutional Repository

Concurrent thermal conductivity measurement and internal structure observation of individual one-dimensional materials using scanning transmission electron microscopy

Li, Dawei
Department of Aeronautics and Astronautics, Kyushu University

Li, Qin-Yi
Department of Aeronautics and Astronautics, Kyushu University

Ikuta, Tatsuya
Department of Aeronautics and Astronautics, Kyushu University

Takahashi, Koji
Department of Aeronautics and Astronautics, Kyushu University

https://hdl.handle.net/2324/4751323

出版情報：Applied Physics Letters. 120 (4), pp.043104-, 2022-01-26. American Institute of Physics : AIP
バージョン：
権利関係：

Applied Physics Letters ACCEPTED MANUSCRIPT
This is the author's peer reviewed, accepted manuscript. However, the online version of record will be different from this version once it has been copyedited and typeset.
PLEASE CITE THIS ARTICLE AS DOI: 10.1063/5.0079153

Concurrent thermal conductivity measurement and internal structure observation of individual one-dimensional materials using scanning transmission electron microscopy

Dawei Li,[1,2] Qin-Yi Li,[1,2,a)] Tatsuya Ikuta,[1,2] Koji Takahashi[1,2]

[1]*Department of Aeronautics and Astronautics, Kyushu University, 744 Motooka, Fukuoka 819-0395, Japan*

[2]*International Institute for Carbon-Neutral Energy Research (WPI-I2CNER), Kyushu University, 744 Motooka, Fukuoka 819-0395, Japan*

Abstract

The thermal conductivity of individual nanomaterials can vary from sample to sample due to the difference in the geometries and internal structures, and thus concurrent structure observation and thermal conductivity measurement at the nanoscale is highly desired but challenging. Here, we have developed an experimental method that allows concurrently the *in-situ* thermal conductivity measurement and the real-time internal structure observation of a single one-dimensional (1D) material using scanning transmission electron microscopy in a scanning electron microscope (STEM-in-SEM). In this method, the two ends of the 1D nanomaterial are bonded on a tungsten probe and a suspended platinum nanofilm, respectively. The platinum nanofilm serves simultaneously as a heater and a resistance thermometer, ensuring highly sensitive thermal measurements. The platinum nanofilm is fabricated on the edge of the silicon wafer so that the electron beam can transmit through the 1D material and be detected by the STEM detector, which caters for real-time observation of the inner nanostructure. Using this method, we *in-situ* measured the thermal conductivities of two cup-stacked carbon nanotubes and concurrently observed the internal hollow structures. We found that the sample with more structural disorders had a lower thermal conductivity. Our measurement method can pave the way to the sample-by-sample elucidation of the structure-property relationship for 1D materials.

[a)]**Author to whom correspondence should be addressed:** qinyi.li@aero.kyushu-u.ac.jp

AIP Publishing

Applied Physics Letters ACCEPTED MANUSCRIPT
This is the author's peer reviewed, accepted manuscript. However, the online version of record will be different from this version once it has been copyedited and typeset.
PLEASE CITE THIS ARTICLE AS DOI: 10.1063/5.0079153
AIP Publishing

Main Text

The relationship between the nanomaterial structure and its thermophysical properties keeps a captivating subject of both fundamental and applied interest since it can not only uncover the nanoscale heat transfer mechanisms but also guide the modulation of the material performance for wide applications including thermal management and thermoelectrics.[1-4] Several experimental methods have been exploited and applied to measure the thermophysical properties of nanomaterials and reveal the microscopic heat transfer mechanisms, represented by the microbridge device method,[5-8] T-type method,[9-12] Raman optothermal method,[13-23] electrical self-heating method,[24-26] and so forth. However, these measurement methods cannot capture the real-time internal structure details of the nanomaterial sample during thermal measurement. Especially for nanowires and nanotubes, usually, the internal structure of the sample is characterized using transmission electron microscopy (TEM) before the thermal measurement. However, the nanomaterial samples from the same batch, and even the different parts of the same individual sample, can often exhibit structural differences, so the separate structural characterization cannot clarify the property-structure relationship. Hence, it is desperately desired to observe the internal structures along with the thermal measurement to gain insight into the relationship between the structure and the thermophysical properties.

In-situ TEM with atomic imaging resolution is a powerful technique to study the structure-property relationship in real time.[27, 28] A series of exciting and impressive efforts have been conducted, however, these endeavors mainly focus on the *in-situ* electrical properties measurement in TEM.[29-31] A few *in-situ* thermal measurements in TEM include the qualitative observation of anisotropic thermal transport in a CNT bundle by monitoring the phase change of gold nanoparticles as thermo-markers,[32] and the nanoscale temperature detection with a well-designed nano-thermocouple assembled in TEM.[33] However, these methods are not suitable for the quantitative thermal conductivity measurement of individual nanomaterials. In 2007, a hot-wire thermal probe for the *in-situ* thermal conductivity measurement of 1D materials in TEM was reported,[34] but the complicated fabrication of the hot-wire

Applied Physics Letters ACCEPTED MANUSCRIPT
This is the author's peer reviewed, accepted manuscript. However, the online version of record will be different from this version once it has been copyedited and typeset.
PLEASE CITE THIS ARTICLE AS DOI: 10.1063/5.0079153
AIP Publishing

probe, the TEM-related assembly, and the difficult TEM operations have so far brought many challenges in the application of this method.

In the present work, we develop an experimental method that facilitates *in-situ* thermal conductivity measurement and internal structure observation of individual 1D materials using scanning transmission electron microscopy in a scanning electron microscope that incorporates the STEM detector into the standard SEM.[35] Despite lower spatial resolution than TEM, STEM-in-SEM is much easier to operate than TEM, and has a much lower accelerating voltage for the electron beam (EB) that can avoid possible damage on the nanomaterial. We applied this method in the *in-situ* thermal conductivity measurement of cup-stacked carbon nanotubes (CNTs), the results of which validated our *in-situ* measurement method. The cup-stacked CNTs have a relatively complicated structure,[36] and the thermal conductivity can depend more significantly on the structure than normal multiwalled CNTs. We observed the internal hollow structure of the cup-stacked CNTs in real time while measuring the thermal conductivity in situ. Our method offers a powerful tool to explore the real-time influence of structures, encapsulation, infusion, deformation, and so forth, on the thermophysical properties.

Figure 1 delineates the schematic diagram of the *in-situ* and real-time thermal conductivity measurement. The two ends of a 1D sample are bonded on a tungsten manipulator probe and a suspended platinum nanofilm by electron-beam induced deposition (EBID), respectively. The *in-situ* thermal conductivity measurement is evolved from the T-type method[9, 10, 34] by comparing the temperature rise of the nanofilm caused by the Joule heating before and after the 1D sample transfer, where the probe equates with the heat sink and the Pt nanofilm serves simultaneously as a heater and a resistance thermometer. Since the calibration of nanofilm properties and our *in-situ* and real-time thermal characterizations are conducted under the high vacuum conditions inside the SEM chamber and the temperature rise is controlled small enough, the effects of both radiation and convection are negligible. The total thermal resistance ($R_{t,tot}$), which includes the thermal resistance of the 1D sample ($l_{1D}/\lambda_{1D}A_{1D}$) and the thermal contact resistance ($R_{t,c}$) between the sensor and the sample, can be extracted

Applied Physics Letters ACCEPTED MANUSCRIPT

AIP Publishing

This is the author's peer reviewed, accepted manuscript. However, the online version of record will be different from this version once it has been copyedited and typeset.

PLEASE CITE THIS ARTICLE AS DOI: 10.1063/5.0079153

as follows,[9, 37]

$$R_{\mathrm{t,tot}} = \frac{l_{\mathrm{1D}}}{\lambda_{\mathrm{1D}} A_{\mathrm{1D}}} + R_{\mathrm{t,c}} = \frac{3\left(\frac{dR_0}{dT_0}\right) l_{\mathrm{s1}}^2 l_{\mathrm{s2}}^2 - l_{\mathrm{s1}} l_{\mathrm{s2}} \left[\left(\frac{dR_0}{dT_0}\right) l_{\mathrm{s}}^2 - 12 A_{\mathrm{s}} \lambda_{\mathrm{s}} l_{\mathrm{s}} \left(\frac{dR}{dP_{\mathrm{s}}}\right)\right]}{A_{\mathrm{s}} \lambda_{\mathrm{s}} l_{\mathrm{s}} \left[\left(\frac{dR_0}{dT_0}\right) l_{\mathrm{s}}^2 - 12 A_{\mathrm{s}} \lambda_{\mathrm{s}} l_{\mathrm{s}} \left(\frac{dR}{dP_{\mathrm{s}}}\right)\right]} \tag{1}$$

where λ_{1D} and A_{1D} are the thermal conductivity and the cross-sectional area of the 1D sample, respectively; l_{1D} is the length of the 1D sample between the two connecting points at the heat sink and the nanofilm; dR_0/dT_0 is the slope of the resistance-temperature relationship of the Pt nanofilm; dR/dP_s is the slope of the relationship between the measured resistance of the Pt nanofilm (R) and Joule power (P_s) after the 1D sample transfer; A_s, λ_s and l_s are the cross-sectional area, the thermal conductivity, and the length of the nanofilm, respectively; l_{s1} and l_{s2} are the lengths of the nanofilm between the junction and the ends of the nanofilm, as depicted in Fig. 1.

We assembled the measurement circuit modules, the STEM detector, and other accessories in the SEM chamber, and utilized the STEM-in-SEM for the concurrent internal structure observation during the thermal conductivity measurement. The details of the experimental setup are provided in the Supplementary Materials. As illustrated in Fig. 1, the suspended nanofilm is deliberately fabricated on the edge of the silicon wafer so that the electron beam can transmit through the 1D sample and the internal structure can be imaged by the STEM detector. See Supplementary Note S1 for the fabrication procedures and SEM images of the suspended platinum nanofilm on the edge of the silicon wafer.

Applied Physics Letters ACCEPTED MANUSCRIPT
This is the author's peer reviewed, accepted manuscript. However, the online version of record will be different from this version once it has been copyedited and typeset.
PLEASE CITE THIS ARTICLE AS DOI: 10.1063/5.0079153
AIP Publishing

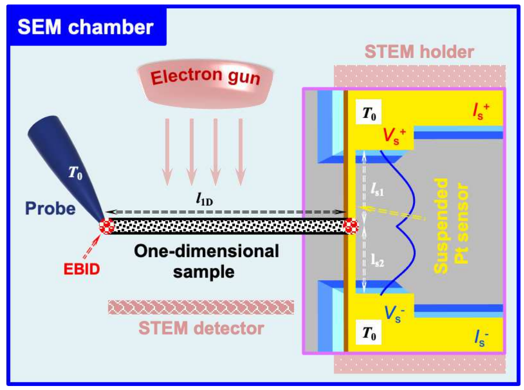

FIG. 1. Schematic illustration of the *in-situ* thermal conductivity measurement method using STEM-in-SEM.

Using this experimental setup, we *in-situ* measured the thermal conductivity of two high-temperature treated cup-stacked CNTs, and concurrently observed the internal structures. See Supplementary Note S2 and S3 for more details about how the samples were picked up and transferred to the measurement devices. The cup-stacked CNT is a chain of truncated graphite cups stacked together, and the graphite cups are tilted a few degrees relative to the longitudinal axis.[36] Figure 2 shows the SEM and STEM images of CNT-a and CNT-b, where the probe, CNT, and the edge of the silicon wafer can be clearly distinguished. Figure 2(c) also presents the typical TEM micrograph of this kind of CNT, in which the cupped wall can be identified. The TEM image was acquired on a TEM (JEM-2100Plus, JEOL) with an electron accelerating voltage of 200 kV. However, the electron accelerating voltages here for SEM and STEM observations were 10 kV and 30 kV, respectively. We have compared the STEM images with different modes and found the high-angle annular dark field (HAADF) mode gives the best imaging performance, where the internal hollow structure of the cup-stacked CNT can be distinguished. The STEM images in this paper are all in the HAADF mode. We measured the outer diameter (D_o) and inner diameter (D_i) of the CNTs from the STEM images. The outer and inner diameters can vary along

Applied Physics Letters ACCEPTED MANUSCRIPT
This is the author's peer reviewed, accepted manuscript. However, the online version of record will be different from this version once it has been copyedited and typeset.
PLEASE CITE THIS ARTICLE AS DOI: 10.1063/5.0079153
AIP Publishing

the length and we measured the diameters at about 50 different locations. D_o and D_i were measured to be 103.0 ± 4.3 nm and 32.9 ± 4.5 nm for CNT-a, and 118.9 ± 8.6 nm and 52.9 ± 8.4 nm for CNT-b. The image brightness of CNT-a is almost uniform in the SEM image in Fig. 2(a), but significantly changes along the length in the STEM image in Fig. 2(b). The dark segment of CNT-a in Fig. 2(b) indicates that the CNT was significantly bent after being transferred to the measurement device, so we had to measure the length of CNT-a from the STEM image before the CNT transfer (Supplementary Fig. S3(a)). In contrast, CNT-b has a uniform image brightness in the STEM image of Fig. 2(e), indicating that CNT-b nearly lies in the same plane. We measured the CNT lengths between the probe and the nanofilm to be 14.5 μm for CNT-a and 10.0 μm for CNT-b. In addition, we can see the white dot-like structural defects or impurities in CNT-a. Thus, on the whole, we observed more structural disorders or non-uniformity in CNT-a than in CNT-b, which can cause a lower thermal conductivity in CNT-a. Note that in the previous SEM-based *in-situ* thermal measurements,[38, 39] it is impossible to *in-situ* measure the inner diameter of the measured segment, not to mention the evaluation of the non-uniformity in the internal structure. The visualization of the internal structure of 1D material during the *in-situ* thermal conductivity measurement is a major achievement in this study.

Applied Physics Letters ACCEPTED MANUSCRIPT

This is the author's peer reviewed, accepted manuscript. However, the online version of record will be different from this version once it has been copyedited and typeset.

PLEASE CITE THIS ARTICLE AS DOI: 10.1063/5.0079153

AIP Publishing

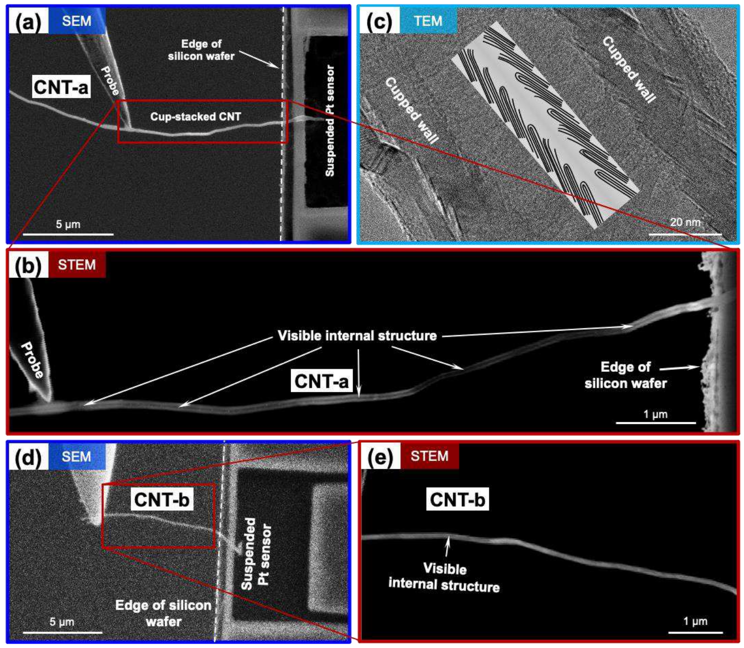

FIG. 2. (a) SEM and (b) STEM images of CNT-a. (c) The typical TEM micrograph of the cup-stacked CNT, which is on the same TEM grid with CNT-a. Inset: schematic illustration of the cup-stacked CNT. (d) SEM and (e) STEM images of CNT-b.

Figure 3 shows the *in-situ* thermal measurement results. Before the CNT transfer, we measured the resistance of the Pt sensor (R) as a function of the Joule power ($P_s = I_s V_s$, where I_s and V_s are the current and voltage, respectively) at different environment temperatures (T_0). Note that the current in this paper only refers to the direct current applied to the nanofilm. In this baseline measurement, we calibrated the resistance-temperature relationship and the thermal conductivity of the Pt nanofilm. The inset of Fig. 3(a) shows the baseline measurement results of the Pt nanofilm used for CNT-a at 278.15 to 318.15 K. By extrapolating the R-P_s curve to zero heating power, we can get the sensor resistance at the environment temperature. Further, from the R-P_s slope, we can calculate the thermal conductivity of the

Applied Physics Letters ACCEPTED MANUSCRIPT

This is the author's peer reviewed, accepted manuscript. However, the online version of record will be different from this version once it has been copyedited and typeset.
PLEASE CITE THIS ARTICLE AS DOI: 10.1063/5.0079153

AIP Publishing

nanofilm using $\lambda_s=(dR_0/dT_0)l_s/[12A_s(dR/dP_s)]$.[9, 34, 40] The suspended Pt nanofilms used for CNT-a and CNT-b are 9.6 μm and 9.7 μm in length, 674.7 nm and 464.3 in width, and 40 nm in thickness. Fig. 3(a) shows the temperature-dependent electrical resistance and thermal conductivity of the nanofilm used for CNT-a. The electrical resistance changes linearly with temperature, and the slope dR_0/dT_0 was 0.213 ±0.003 Ω/K. Figure 3(b) shows the change in the resistance of the nanofilm ($\Delta R = R-R_0$) as a function of the Joule power in the baseline measurement and after CNT-a transfer. The corresponding results for CNT-b are provided in Supplementary Fig. S4. The slope dR_0/dT_0 of the nanofilm used for CNT-b was 0.289 ±0.003 Ω/K. To eliminate the heating effect of the electron beam, we turned off the electron beam when we conducted the thermal conductivity measurement. Compared with the baseline measurement, the change in the resistance of the nanofilm decreased after being bonded with the CNT samples, since part of the heat flux went through the CNT to the heat sink (*i.e.* the tungsten probe) and the average temperature rise of the nanofilm decreased. Based on the obtained dR_0/dT_0, the average temperature rise of the nanofilm (θ) was obtained as $\theta = \Delta R/(dR_0/dT_0)$. Figure 3(c) illustrates the difference in the average temperature rise of the Pt nanofilm after the CNT transfer and baseline measurement ($\theta - \theta_{BL}$), which clearly reveals the difference. Using Eq. (1), we measured the total thermal resistance for CNT-a and CNT-b to be $(8.9 \pm 5.0)\times10^7$ K/W and $(3.3 \pm 0.4)\times10^7$ K/W, respectively. Although we cannot separate the thermal contact resistance ($R_{t,c}$) in our measurement, $R_{t,c}$ is negligible as reported in the literature with similar contact conditions,[8, 9, 34, 41] since we bonded the CNT firmly with the sensor and the heat sink using EBID. Thus, we took $R_{t,c}$ in Eq. (1) as 0 and calculated the thermal conductivities which here correspond to the lower bound of the actual thermal conductivities. Here we used the shell cross-sectional area of the CNT for the thermal conductivity calculation, which is the same as the previous measurements on cup-stacked CNTs.[41, 42] As shown in Fig. 3(c), the thermal conductivity of CNT-a and CNT-b are 21.7 ± 12.4 W/m·K and 33.8 ± 8.0 W/m·K, respectively, which approximately fall in the range of the reported thermal conductivity of this kind of cup-stacked CNT in previous measurements.[41, 42] Our uncertainty analysis is provided in Supplementary Note S6. It should be pointed out that the

Applied Physics Letters ACCEPTED MANUSCRIPT
This is the author's peer reviewed, accepted manuscript. However, the online version of record will be different from this version once it has been copyedited and typeset.
PLEASE CITE THIS ARTICLE AS DOI: 10.1063/5.0079153
AIP Publishing

previous measurements in Ref. 42 did not provide the uncertainty, while the uncertainty reported in Ref. 41 could be underestimated. The thermal conductivity of cup-stacked CNTs is dominated by the interfacial thermal resistance between graphene or graphite cups, which can be affected by structural bending and disorders. The thermal conductivity difference between CNT-a and CNT-b can be explained by the structural difference observed in the STEM images as discussed earlier, as well as the sample variation in the crystallization defect levels that cannot be observed with STEM-in-SEM.

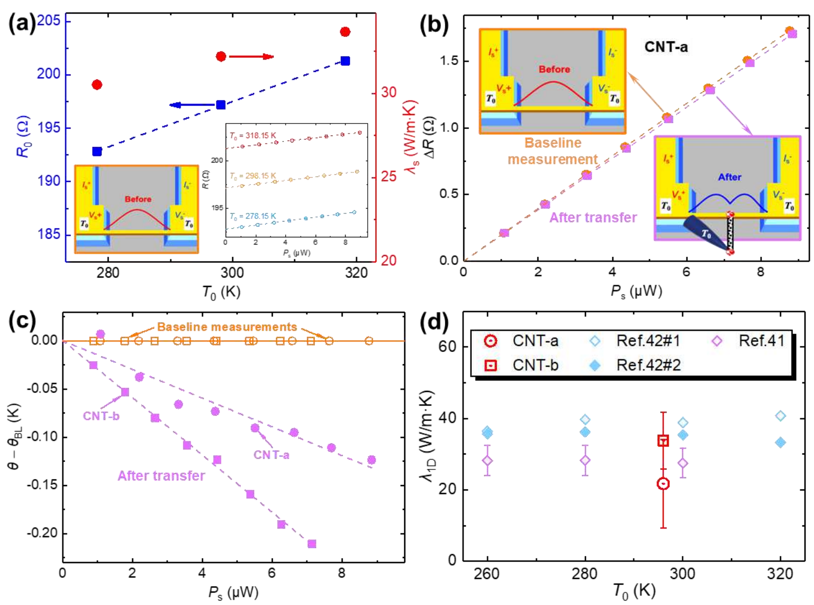

FIG. 3. (a) The temperature dependence of the resistance at zero heating power, and the thermal conductivity, of the Pt nanofilm before transferring CNT-a. Inset: the baseline measurement results for the relationship between the resistance of the nanofilm and the Joule heating power. (b) The change in the resistance of the nanofilm as a function of the Joule power in the baseline measurement and after CNT-a transfer. (c) The difference in the average temperature rise of the nanofilm after the CNT transfer and baseline measurement. (d) The thermal conductivities of

Applied Physics Letters ACCEPTED MANUSCRIPT
This is the author's peer reviewed, accepted manuscript. However, the online version of record will be different from this version once it has been copyedited and typeset.
PLEASE CITE THIS ARTICLE AS DOI: 10.1063/5.0079153
AIP Publishing

CNT-a and CNT-b plotted with the literature results.

One concern about our method is whether the electron beam can damage the sample, since the electron beam can introduce defects in graphene.[43] Actually, for multi-walled nanotubes or nanowires, the electron-beam-induced damage is negligible under TEM observation where the acceleration voltage is normally 200 kV or 300 kV.[36, 44, 45] In our work, the acceleration voltage of STEM-in-SEM observation is 30 kV, which is much lower than TEM and ensures the sample safety. Besides, the data was stable during the measurement, which also confirmed the negligible electron-beam effect. We also evaluated the heating effect of the electron beam irradiation by monitoring the temperature change in the Pt sensor. From Fig. S5, we found that the electron beam does heat the sample and the temperature change caused by the EB irradiation is less than 0.6 K. To avoid the EB heating effect, we turned off the EB when we conducted the thermal conductivity measurement of the CNTs, so the EB irradiation does not affect the thermal conductivity results. In the future, because the movement of the silicon wafer and the probe are independently controlled by the SEM stage and the manipulator, we can also introduce deformation by moving the probe and study the effect of deformation on the properties.

In conclusion, we have developed an experimental method that enables concurrent thermal conductivity measurement and internal structure observation of single 1D materials using STEM-in-SEM. Utilizing this setup, we observed the internal non-uniform structures of the cup-stacked CNTs and measured the thermal conductivity in situ. The thermal conductivity results fall in the range of the previously reported values, while the thermal conductivity difference between our measured samples can be attributed to the structural difference. Our experimental method can find wide applications in the sample-by-sample elucidation of the structure-property correlation for 1D materials in real time.

Supplementary Material

See supplementary material for further details on the fabrication procedures of the suspended

Applied Physics Letters ACCEPTED MANUSCRIPT
This is the author's peer reviewed, accepted manuscript. However, the online version of record will be different from this version once it has been copyedited and typeset.
PLEASE CITE THIS ARTICLE AS DOI: 10.1063/5.0079153
AIP Publishing

platinum nanofilm on the edge of the silicon wafer, practical images of the experimental setup for the *in-situ* and real-time thermal characterization, thermal measurement results of CNT-b, the tests on the effects of the electron beam irradiation and the current applied to the nanofilm sensor on thermal characterization and the uncertainty analysis.

Acknowledgments

This work was supported by JSPS KAKENHI (Grant Nos. JP20H02090 and JP21K18693) and JST CREST (Grant No. JPMJCR18I1). We acknowledge Prof. Yasuyuki Takata for providing the FEI Versa 3D DualBeam instrument. D. Li thanks China Scholarship Council for the financial support.

Data Availability

The data that supports the findings of this study are available within the article and the supplementary material.

Applied Physics Letters ACCEPTED MANUSCRIPT
This is the author's peer reviewed, accepted manuscript. However, the online version of record will be different from this version once it has been copyedited and typeset.
PLEASE CITE THIS ARTICLE AS DOI: 10.1063/5.0079153
AIP Publishing

References

1. A. M. Marconnet, M. A. Panzer and K. E. Goodson, Rev. Mod. Phys. **85** (3), 1295-1326 (2013).
2. E. Pop, V. Varshney and A. K. Roy, MRS Bull. **37** (12), 1273-1281 (2012).
3. Y. Xu, Z. Y. Li and W. H. Duan, Small **10**, 2182-2199 (2014).
4. Q.-Y. Li, Q. Hao, T. Zhu, M. Zebarjadi and K. Takahashi, Eng. Sci. **13**, 24-50 (2021).
5. P. Kim, L. Shi, A. Majumdar and P. L. McEuen, Phys. Rev. Lett. **87** (2001).
6. L. Shi, D. Y. Li, C. H. Yu, W. Y. Jang, D. Kim, Z. Yao, P. Kim and A. Majumdar, J. Heat. Trans-T. ASME. **125**, 881-888 (2003).
7. T. Kodama, M. Ohnishi, W. Park, T. Shiga, J. Park, T. Shimada, H. Shinohara, J. Shiomi and K. E. Goodson, Nature Mater. **16**, 892-897 (2017).
8. J. Kim, E. Fleming, Y. Zhou and L. Shi, J. Phys. D: Appl. Phys. **51** (10), 103002 (2018).
9. M. Fujii, X. Zhang, H. Q. Xie, H. Ago, K. Takahashi, T. Ikuta, H. Abe and T. Shimizu, Phys. Rev. Lett. **95**, 065502 (2005).
10. T. Miao, S. Shi, S. Yan, W. Ma, X. Zhang, K. Takahashi and T. Ikuta, J. Appl. Phys. **120**, 124302 (2016).
11. M. Narasaki, Q. Y. Li, T. Ikuta, J. Miyawaki and K. Takahashi, Carbon **153**, 539-544 (2019).
12. J. Hirotani, T. Ikuta, T. Nishiyama and K. Takahashi, Nanotechnology **22**, 315702 (2011).
13. A. A. Balandin, S. Ghosh, W. Z. Bao, I. Calizo, D. Teweldebrhan, F. Miao and C. N. Lau, Nano Lett. **8**, 902-907 (2008).
14. W. Cai, A. L. Moore, Y. Zhu, X. Li, S. Chen, L. Shi and R. S. Ruoff, Nano Lett. **10**, 1645-1651 (2010).
15. C. Faugeras, B. Faugeras, M. Orlita, M. Potemski, R. R. Nair and A. K. Geim, ACS Nano **4** (4), 1889-1892 (2010).
16. J. U. Lee, D. Yoon, H. Kim, S. W. Lee and H. Cheong, Phys. Rev. B **83** (8) (2011).

Applied Physics Letters ACCEPTED MANUSCRIPT
This is the author's peer reviewed, accepted manuscript. However, the online version of record will be different from this version once it has been copyedited and typeset.
PLEASE CITE THIS ARTICLE AS DOI: 10.1063/5.0079153
AIP Publishing

17. S. S. Chen, Q. Z. Wu, C. Mishra, J. Y. Kang, H. J. Zhang, K. J. Cho, W. W. Cai, A. A. Balandin and R. S. Ruoff, Nature Mater. **11**, 203-207 (2012).

18. Q.-Y. Li, K. Takahashi and X. Zhang, Int. J. Heat Mass Transfer **134**, 539-546 (2019).

19. A. R. Fan, Q. Y. Li, W. G. Ma and X. Zhang, J. Nanosci. Nanotechnol. **19** (11), 7004-7013 (2019).

20. Q. Y. Li, K. Katakami, T. Ikuta, M. Kohno, X. Zhang and K. Takahashi, Carbon **141**, 92-98 (2019).

21. Q.-Y. Li, K. Xia, J. Zhang, Y. Zhang, Q. Li, K. Takahashi and X. Zhang, Nanoscale **9** (30), 10784-10793 (2017).

22. Q. Y. Li and X. Zhang, Thermochim. Acta **581**, 26-31 (2014).

23. Q.-Y. Li, X. Zhang and K. Takahashi, Int. J. Heat Mass Transfer **125**, 1230-1239 (2018).

24. Q. Y. Li, K. Takahashi, H. Ago, X. Zhang, T. Ikuta, T. Nishiyama and K. Kawahara, J. Appl. Phys. **117** (2015).

25. S. N. Raja, R. Rhyner, K. Vuttivorakulchai, M. Luisier and D. Poulikakos, Nano Lett. **17** (1), 276-283 (2017).

26. Q.-Y. Li, T. Feng, W. Okita, Y. Komori, H. Suzuki, T. Kato, T. Kaneko, T. Ikuta, X. Ruan and K. Takahashi, ACS Nano **13**, 9182-9189 (2019).

27. W. Li, M. Li, X. Q. Wang, P. C. Xu, H. T. Yu and X. X. Li, Nano Today **35** (2020).

28. G. Divitini, S. Cacovich, F. Matteocci, L. Cina, A. Di Carlo and C. Ducati, Nat Energy **1** (2016).

29. T. Hayashi, T. C. O'Connor, K. Higashiyama, K. Nishi, K. Fujisawa, H. Muramatsu, Y. A. Kim, B. G. Sumpter, V. Meunier, M. Terrones and M. Endo, Nanoscale **5** (21), 10212-10218 (2013).

30. C. Zhang, M. Neklyudova, L. Fang, Q. Xu, H. Wang, F. D. Tichelaar and H. W. Zandbergen, Nanotechnology **26** (15) (2015).

31. A. Barreiro, F. Bornert, S. M. Avdoshenko, B. Rellinghaus, G. Cuniberti, M. H. Rummeli and L. M. K. Vandersypen, Scientific Reports **3** (2013).

32. H. Hamasaki, S. Takimoto and K. Hirahara, Nano Lett. **21** (7), 3134-3138 (2021).

33. N. Kawamoto, Y. Kakefuda, I. Yamada, J. Yuan, K. Hasegawa, K. Kimoto, T. Hara, M. Mitome,

Applied Physics Letters ACCEPTED MANUSCRIPT
This is the author's peer reviewed, accepted manuscript. However, the online version of record will be different from this version once it has been copyedited and typeset.
PLEASE CITE THIS ARTICLE AS DOI: 10.1063/5.0079153
AIP Publishing

Y. Bando, T. Mori and D. Golberg, Nano Energy **52**, 323-328 (2018).

34. C. Dames, S. Chen, C. T. Harris, J. Y. Huang, Z. F. Ren, M. S. Dresselhaus and G. Chen, Rev. Sci. Instrum. **78**, 104903 (2007).
35. T. Klein, E. Buhr and C. Georg Frase, in *ADIEP*, edited by P. W. Hawkes (Elsevier, 2012), Vol. 171, pp. 297-356.
36. M. Endo, Y. A. Kim, T. Hayashi, Y. Fukai, K. Oshida, M. Terrones, T. Yanagisawa, S. Higaki and M. S. Dresselhaus, Appl. Phys. Lett. **80**, 1267-1269 (2002).
37. Q.-Y. Li, K. Takahashi and X. Zhang, Phys. Rev. Lett. **119** (17), 179601 (2017).
38. J. Hirotani, T. Ikuta and K. Takahashi, Int. J. Thermophys. **34**, 2351-2360 (2013).
39. H. Wang, K. Kurata, T. Fukunaga, H. Takamatsu, X. Zhang, T. Ikuta, K. Takahashi, T. Nishiyama, H. Ago and Y. Takata, Scientific Reports **6** (1), 21823 (2016).
40. T. Miao, D. Li, X. Wang, W. Ma and X. Zhang, Phys. Rev. B **100**, 235402 (2019).
41. Y. Yamada, A. Askounis, T. Ikuta, K. Takahashi, Y. Takata and K. Sefiane, J. Appl. Phys. **121**, 15104 (2017).
42. K. Takahashi, Y. Ito, T. Ikuta, X. Zhang and M. Fujii, Physica B-Condensed Matter **404** (16), 2431-2434 (2009).
43. H. Malekpour, P. Ramnani, S. Srinivasan, G. Balasubramanian, D. L. Nika, A. Mulchandani, R. K. Lake and A. A. Balandin, Nanoscale **8** (30), 14608-14616 (2016).
44. Y. Tomo, A. Askounis, T. Ikuta, Y. Takata, K. Sefiane and K. Takahashi, Nano Lett. **18**, 1869-1874 (2018).
45. Q. Y. Li, R. Matsushita, Y. Tomo, T. Ikuta and K. Takahashi, J. Phys. Chem. Lett. **10**, 3744-3749 (2019).

This is the author's peer reviewed, accepted manuscript. However, the online version of record will be different from this version once it has been copyedited and typeset.

PLEASE CITE THIS ARTICLE AS DOI: 10.1063/5.0079153

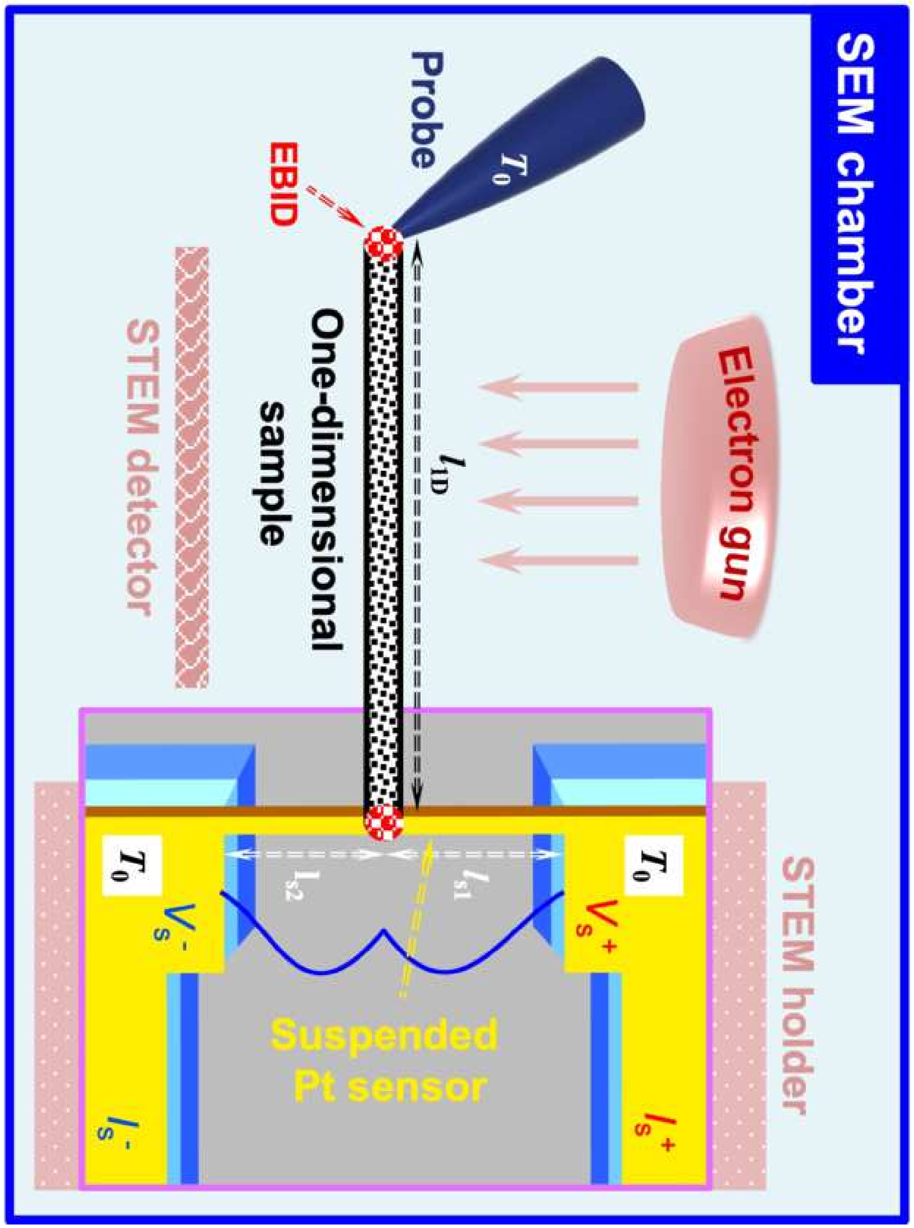

ACCEPTED MANUSCRIPT
Applied Physics Letters
This is the author's peer reviewed, accepted manuscript. However, the online version of record will be different from this version once it has been copyedited and typeset.
PLEASE CITE THIS ARTICLE AS DOI: 10.1063/5.0079153
AIP Publishing

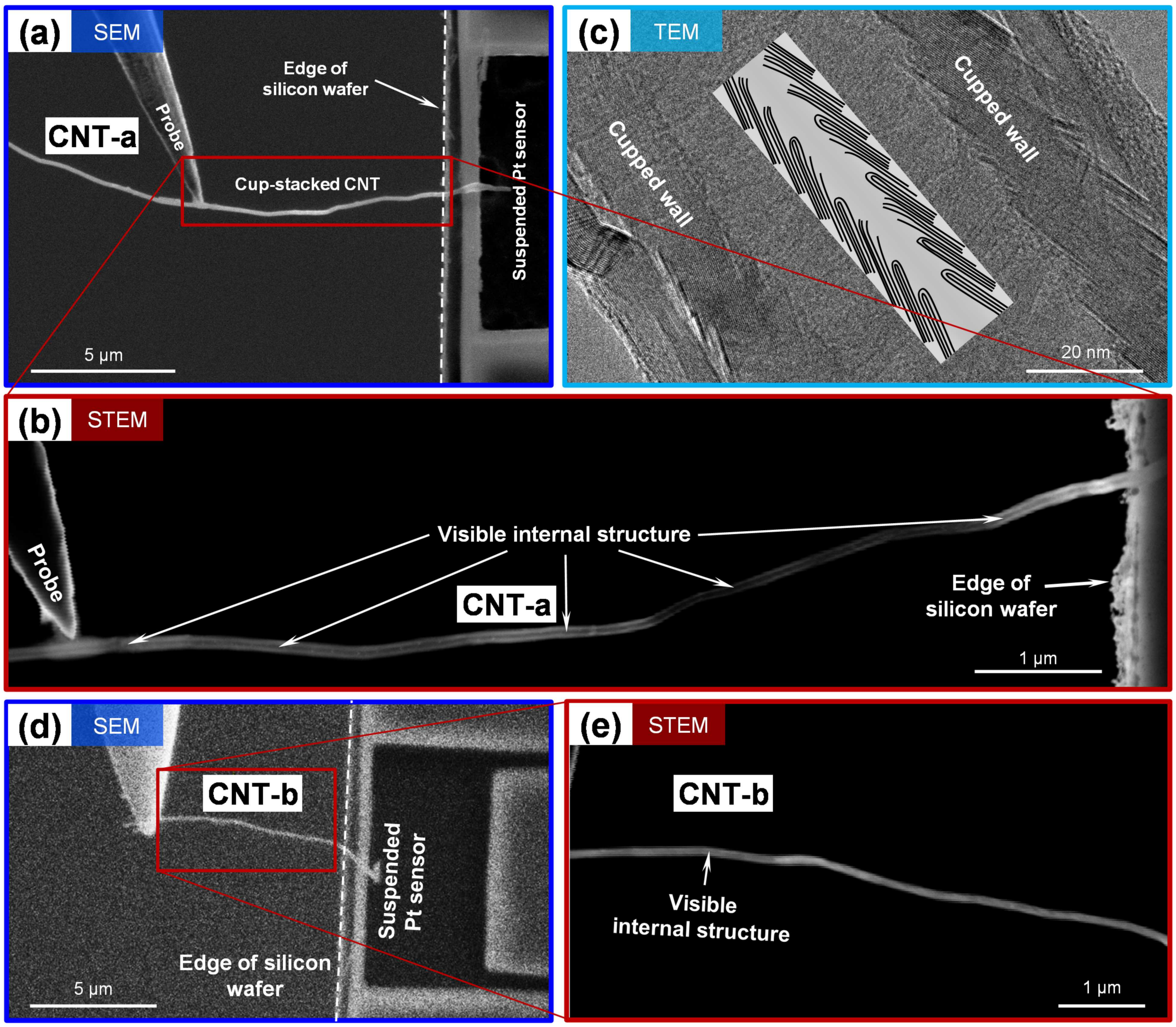

Applied Physics Letters ACCEPTED MANUSCRIPT
This is the author's peer reviewed, accepted manuscript. However, the online version of record will be different from this version once it has been copyedited and typeset.
PLEASE CITE THIS ARTICLE AS DOI: 10.1063/5.0079153
AIP Publishing